HHS Public Access

Author manuscript

Int J Ind Ergon. Author manuscript; available in PMC 2021 September 21.

Published in final edited form as:

Int J Ind Ergon. 2020 May ; 77: . doi:10.1016/j.ergon.2020.102946.

Identification of effective engineering methods for controlling handheld workpiece vibration in grinding processes

Ren G. Dong[*], **Daniel E. Welcome**, **Xueyan S. Xu**, **Thomas W. McDowell**

Physical Effects Research Branch, Health Effects Laboratory Division National Institute for Occupational Safety and Health, Morgantown, WV, 26505, USA

Abstract

The objective of this study is to identify effective engineering methods for controlling handheld workpiece vibration during grinding processes. Prolonged and intensive exposures to such vibration can cause hand-arm vibration syndrome among workers performing workpiece grinding, but how to effectively control these exposures remains an important issue. This study developed a methodology for performing their analyses and evaluations based on a model of the entire grinding machine-workpiece-hand-arm system. The model can simulate the vibration responses of a workpiece held in the worker's hands and pressed against a grinding wheel in order to shape the workpiece in the major frequency range of concern (6.3–1600 Hz). The methodology was evaluated using available experimental data. The results suggest that the methodology is acceptable for these analyses and evaluations. The results also suggest that the workpiece vibration resulting from the machine vibration generally depends on two mechanisms or pathways: (1) the direct vibration transmission from the grinding machine; and (2) the indirect transmission that depends on both the machine vibration transmission to the workpiece and the interface excitation transformation to the workpiece vibration. The methodology was applied to explore and/or analyze various engineering methods for controlling workpiece vibrations. The modeling results suggest that while these intervention methods have different advantages and limitations, some of their combinations can effectively reduce the vibration exposures of grinding workers. These findings can be used as guidance for selecting and developing more effective technologies to control handheld workpiece vibration exposures.

Keywords

Hand-arm vibration; Hand-transmitted vibration; Handheld workpiece vibration; Vibration control

[*]Corresponding author. PERB/HELD/NIOSH/CDC 1095 Willowdale Road, MS L-2027, Morgantown, WV, 26505, USA. rkd6@cdc.gov (R.G. Dong).

Appendix A. Supplementary data

The data reported in this article are availble upon request. https://doi.org/10.1016/j.ergon.2020.102946https://doi.org/10.1016/j.ergon.2020.102946.

1. Introduction

Prolonged and intensive vibration exposure often affects workers performing the grinding of handheld workpieces in manufacturing some parts of sports equipment and furniture, fabricating denture parts, and sharpening tool cutting or drilling bits (Ikeda et al., 1998; Kaulbars, 2014; Chen et al., 2015). Such vibration exposure may cause vibration-induced white finger or hand-arm vibration syndrome but effective control of the exposure remains an important issue (Chen et al., 2015; Griffin, 1990). We have launched a systematic investigation to help control such vibration exposures. As the first step of the investigation, a series of experimental studies at a workplace were conducted to identify the basic vibration characteristics of the workpiece held in the worker's hands and pressed against a grinding wheel in order to shape the workpiece (Chen et al., 2017). In these studies, the vibrations from 6.3 to 1600 Hz in the one-third octave bands on workpieces and grinding machines were simultaneously measured. This study has led to the proposal of a combination of management, engineering, and personal protection methods for controlling hand-transmitted vibration exposures (Dong et al., 2016). As the second step of the investigation, the vibration responses of the workpiece-hand-arm system were simulated and measured in a laboratory (Xu et al., 2018). The results were used to develop a model of the grinding machine-workpiece-hand-arm system (Dong et al., 2018), which is applicable for predicting the system vibration responses from 6.3 to 1600 Hz. The next step is to apply the model to analyze and identify effective and practical engineering intervention methods for controlling handheld workpiece vibration.

It has been confirmed that the vibration of handheld workpieces in their grinding processes results partially from the vibration generated on and transmitted from the grinding machine and partially from the grinding/abrasive process at the workpiece interface (Chen et al., 2017; Tönshoff and Degenhardt, 1982). Therefore, the basic engineering strategy for controlling the vibration exposure is to control the two sources of vibrations and to minimize the responses of workpiece and the vibration transmission to the hands of workers (Chen et al., 2017; Dong et al., 2016). While it is beyond the scope of this study to address all of the approaches, the current study primarily examined the approaches for controlling the workpiece responses to these two vibration sources and the vibration transmission to the hands. Although such approaches have been implemented in the design of some grinding machines and in some practices at workplaces (https://www.google.com/se, 1120; https://www.familyhandyma, 2020; https://www.youtube.com/w, 2020), their theoretical foundations have not been well established and understood, as many of the implemented methods and practices were not originally or intentionally designed to reduce the vibration exposure. As a result, some of the designs and practices may increase vibration exposures (HSE, 2005). Because each of the intervention methods may have different requirements, conditions, and/or useful frequency ranges for them to work effectively, it is important to enhance the understanding of them and to identify the application requirements so that they can be appropriately selected, improved, and applied. Further studies are also required to develop other effective engineering intervention methods and technologies for controlling handheld workpiece vibration exposures.

A methodology for analyzing and evaluating these engineering intervention methods has not been well established. Although the analyses can be partially performed using the model of the workpiece-handarm system developed in the previous study (Dong et al., 2018), it remains unclear how to effectively consider both types of vibration sources in the analyses. Furthermore, there are usually some interactions between the two types of vibration sources, according to the findings of the studies on other types of workpiece grinding (Oryński and Pawłowski, 1999; Hahn and Lindsay, 1970; Oliveira et al., 2008; Aurich et al., 2009). It is unclear how to consider these interactions in the analyses. Therefore, the specific aims of the study are as follows: (1) to refine the model, further validate it, and to extend it so that it can be used to analyze various engineering methods for controlling workpiece vibration; and (2) to formulate a methodology for the analyses and validate it; and (3) to apply the methodology to analyze and evaluate some available and potential intervention methods. The results were discussed and used to identify the effectiveness, advantages, and limitations of the intervention methods.

2. Methods

2.1. The system models and workpiece vibration responses

Fig. 1(a) shows a pictorial view of a typical belt grinding procss of a workpiece (golf club head) held by two hands on a belt grinding machine observed at a workplace (Chen et al., 2017). The possible vibration sources and their hypothesized transmission pathways are illustrated in Fig. 1(b). The basic model of the entire machine-workpiece-hand-arm system used in the current study is illustrated in Fig. 1(c), which was developed in a previous study (Dong et al., 2018). Because additional components must be considered to analyze some of the engineering intervention methods, the basic model was extended to include these components. The specific extensions, together with their associated intervention methods, are described in Section 2.3. For the purpose of this study, six test treatments were considered in the basic modeling analyses, which are the combinations of bare-hand operations with two feed forces (15 N and 30 N) on three different grinding interfaces (R45, R55, and R65). The model parameters for each of the six treatments are listed in Table 1. Different from the reported model parameters that were calibrated using experimental data measured on assumed laboratory grinding interfaces (Xu et al., 2018; Dong et al., 2018), the parameters listed in Table 1 were calibrated in the current study using a set of reported human subject experimental data measured using three real interface sections cut from the drive wheels of belt grinding machines at a workplace (Dong et al., 2018). The parameter calibration method used in the current study was the same as that developed and used in the previously-reported study (Dong et al., 2018).

The equation of motion for the system model of each intervention method was generally expressed as follows:

$$[\boldsymbol{M}]\left\{\ddot{\boldsymbol{Z}}\right\} + [\boldsymbol{C}]\left\{\dot{\boldsymbol{Z}}\right\} + [\boldsymbol{K}]\left\{\boldsymbol{Z}\right\} = \left\{\boldsymbol{F}\right\} \quad (1)$$

This equation was used to calculate the system displacement responses (***z***) to each of the two force excitations (***F***): $\boldsymbol{F}_W = F_W \exp^{j\omega t}$ and $\boldsymbol{F}_C = F_C \exp^{j\omega t}$, in which $j = \sqrt{-1}$, ω is angular frequency, and t is time.

When the machine vibration excitation ($\boldsymbol{F}_W$) was considered, the calculated responses were used to determine the conventional workpiece vibration transfer function ($\boldsymbol{T}_W$) using the workpiece response ($\boldsymbol{z}_c$) and drive wheel response ($\boldsymbol{z}_W$):

$$\boldsymbol{T}_W = \boldsymbol{z}_c / \boldsymbol{z}_w = \boldsymbol{A}_{C-W} / \boldsymbol{A}_W, \tag{2}$$

where $\boldsymbol{A}_W$ ($= -\omega^2 \boldsymbol{z}_w$) is the drive wheel vibration acceleration, and $\boldsymbol{A}_{C\text{-}W}$ ($= -\omega^2 \boldsymbol{z}_c$) is the workpiece vibration acceleration resulting from the machine vibration acting on the drive wheel.

When the interface vibration force ($\boldsymbol{F}_C$) was used as the input, the resulting acceleration response ($\boldsymbol{A}_{C\text{-}C}$) was used to define a new transfer function ($\boldsymbol{T}_C$) as follows:

$$\boldsymbol{T}_C = \boldsymbol{A}_{C-C} / (\boldsymbol{F}_C / \boldsymbol{m}_c) \tag{3}$$

The force-mass ratio ($\boldsymbol{F}_C / m_c$) in this equation is the acceleration of the workpiece that is free or not constrained in any system but subjected to the same vibration force ($\boldsymbol{F}_C$) as that generating the system responses. Therefore, this transfer function represents the normalization of the vibration acceleration of the workpiece constrained in the system with respect to the free workpiece acceleration resulting from the same excitation force. It provides a dimensionless measure of the efficiency of the force-motion transformation in the frequency domain; it is reasonable to term this transfer function as force-motion transfer function.

As the phase angles of these transfer functions were not of concern in this study, only the magnitudes of the two transfer functions ($T_W = |\boldsymbol{T}_W|$; $T_C = |\boldsymbol{T}_C|$) were quantified and used in this study, which were referred to as transmissibility in the following presentations. For the same reason, only the magnitude of the system vibration was considered in this study.

2.2. An approximate method for estimating workpiece vibration from grinding machine vibration

We hypothesize that these two vibration transmissibility spectra can be used as a basis to evaluate the engineering intervention methods for controlling the workpiece vibration and its transmission to the human hands. The hypothesis was tested in this study, together with the test of the hypothesized vibration transmission pathway shown in Fig. 1(b), through the development and test of an approximation method for estimating workpiece vibration from grinding machine vibration. According to the flowchart shown in Fig. 1(b), the vibration on the drive wheel should be used to represent the machine vibration. Unfortunately, it is very difficult to measure the drive wheel vibration. Alternatively, the vibration on the grinding machine body near the grinding drive wheel was measured in the previous study (Chen et al., 2017). It was used in the current study to represent the machine vibration. Because the peak frequencies of the machine vibration were correlated with those measured on the

workpieces in the frequency range of 20–125 Hz (Chen et al., 2017), it is reasonable to assume that the machine body vibration (A_{MB}) is correlated with the drive wheel vibration (A_W) in this frequency range, as the drive wheel is located between the machine body and workpiece. Then, their linear regression relationship can be expressed as follows:

$$A_W \approx \chi A_{MB}, \tag{4}$$

where χ is the regression slope/coefficient. According to Eq. (2), the workpiece vibration magnitude ($A_{C\text{-}W}$) resulting from the drive wheel vibration can be estimated as follows:

$$A_{C-W} \approx T_W A_W \approx T_W(\chi A_{MB}) \tag{5}$$

As also illustrated in Fig. 1(b), besides directly producing the workpiece vibration, the vibration transmitted to the grinding interface can also serve as a geometric input to cause the vibration of the interface cutting force (Hahn and Lindsay, 1970; Oliveira et al., 2008; Aurich et al., 2009). While the cutting vibration force ($F_{C\text{-}W}$) resulting from the transmitted vibration may be complex, it is reasonable to hypothesize that the resulting cutting vibration force is correlated with the transmitted vibration, or their regression relationship can be expressed as follows:

$$F_{C-W} \approx \zeta A_{C-W} \approx \zeta T_W \chi A_{MB} \tag{6}$$

where ζ is their regression slope/coefficient. According to Eq. (3), the resulting additional workpiece vibration ($A_{C\text{-}CW}$) can be written as follows:

$$A_{C-CW} \approx T_C(F_{C-W}/m_c) \approx (\zeta\chi/m_c)T_C T_W A_{MB} \tag{7}$$

Then, the total workpiece vibration ($A_{C\text{-}M}$) resulting from the machine vibration is the sum of these two types of vibrations or it can be expressed as follows:

$$A_{C-M} \approx A_{C-W} + A_{C-CW} \approx \chi T_W A_{MB}\left[1 + \left(\frac{\zeta}{m_c}\right)T_C\right] \tag{8}$$

This approximation method was tested using the experimental data measured in a previous study (Chen et al., 2017). A series of analyses were performed to examine the correlations among the measured machine body vibration, the estimated vibrations at different stages, and the measured workpiece vibration ($A_{C\text{-}Measured}$). The results are presented in section 3.3.

2.3. Modeling analyses of the methods for reducing workpiece vibration

The results presented in Section 3.3 support the hypothesis that the two types of transmissibility (T_W and T_C) can be used to represent the frequency responses of the workpiece to the two excitations for assessing the effectiveness of any intervention method for controlling the vibration transmission. Therefore, they were calculated for each of the analyzed vibration control methods and used as a basis for assessing their effectiveness. If not specified, the basic model shown in Fig. 1(c) was used in the analyses.

2.3.1. Predicting the effects of the interface dynamic properties on workpiece vibration—The interface dynamic properties are represented by the interface stiffness (K_1) and damping value (C_1) shown in Fig. 1. As presented in Table 1, the damping value of the tested sample sections of the synthetic rubber interface wheels increased with the increase in the stiffness of the samples. To simplify the analyses for understanding their basic effects on the workpiece vibration, we assumed that these two interface properties could vary by the same percentage (α) of reference interface stiffness ($K_{1\text{-Ref}}$) and damping value (C_1) or

$$K_{1-\alpha} = \alpha \cdot K_{1-\text{Ref}}, \quad C_{1-\alpha} = \alpha \cdot C_{1-\text{Ref}} \tag{9}$$

While the machine vibration (F_W) can remain unchanged in the prediction of $T_{W\text{-}\alpha}$, the cutting vibration force ($F_{C\text{-}\alpha}$) should be reduced with the reduction of the interface stiffness and damping value (Tönshoff and Degenhardt, 1982; Oryński and Pawłowski, 1999; Hahn and Lindsay, 1970; Oliveira et al., 2008). The specific influence is complex, as the cutting vibration force may depend on many factors such as abrasive material and grain size, workpiece material, grinding speed, feed force, interface geometries, vibration frequency, interface temperature. However, reducing the interface stiffness should generally decrease the cutting vibration force if the other grinding conditions remain unchanged. It is not the purpose of the current study to simulate the detailed grinding process or interactions for a specific case; the study's purpose is to qualitatively understand the basic effects of the interface dynamic properties on the workpiece vibration. Thus, we assumed that the reduced cutting vibration force was associated with the percentage change (α) of the interface properties as follows:

$$|F_{C-\alpha}| = \alpha^{\beta} \cdot |F_{C-\text{Ref}}| \tag{10}$$

where β is the association index, and $F_{C\text{-Ref}}$ is the reference excitation force. The reference force was taken as 1 N for any case in this study. For a direct comparison, the force-motion transmissibility for a changed interface ($T_{C\text{-}\alpha}$) was determined by normalizing the acceleration ($A_{C\text{-}\alpha}$) calculated with $F_{C\text{-}\alpha}$ with respect to the original free workpiece acceleration or

$$T_{C-\alpha} = A_{C-\alpha}/(F_{C-\text{Ref}}/m_c) \tag{11}$$

2.3.2. Predicting the effects of workpiece adapters on vibration exposure—If the adapter is sufficiently rigid in the frequency range of concern, and it is tightly attached to the workpiece, the effect of the adapter on the workpiece vibration can be predicted by replacing m_c in the basic model with $m_{c\text{-}\lambda}$ expressed as follows:

$$m_{c-\lambda} = \lambda \cdot m_c, \quad \lambda = (m_{ad} + m_c)/m_c, \tag{12}$$

where m_{ad} is the adapter mass. To directly compare the adapter/workpiece transfer function with the original T_C, the new transfer function, $T_{C\text{-}\lambda}$, was calculated using the acceleration response ($A_{C\text{-}\lambda}$) for each $m_{c\text{-}\lambda}$ and the original free workpiece acceleration or

$$T_{C-\lambda} = A_{C-\lambda}/(F_{C-Ref}/m_c) \quad (13)$$

A vibration absorber may be installed on the adapter to further reduce the workpiece vibration in a certain frequency range. As shown in Fig. 2(a), the absorber was simulated as a lumped mass element (m_{ab}) connected to the adapter mass (m_{ad}) through a set of spring-damping elements (K_{ab}, C_{ab}), which were added to the basic system model shown in Fig. 1(c). Similar to that shown in Eq. (13), the $T_{c\text{-}\gamma}$ for each adapter-absorber combination (γ) was calculated using the workpiece acceleration response ($A_{C\text{-}\gamma}$) predicted with the revised model shown in Fig. 2(a) and the original free workpiece acceleration, or

$$T_{C-\gamma} = A_{C-\gamma}/(F_{C-Ref}/m_c) \quad (14)$$

Alternatively, the adapter can be connected to the workpiece using some viscous-elastic material, which may isolate some vibration from transmission to the hands, similar to the function of a suspended handle. This was simulated using a revised additional model shown in Fig. 2(b). With the system responses (z_{ad}, z_w, A_{ad}, …) predicted using the revised model, the hand vibration exposure can be represented using the vibration transmissibility of the adapter subjected to the machine vibration ($T_{W\text{-}ad}$) and that subjected to the grinding interface excitation ($T_{C\text{-}ad}$), which can be calculated using the following formulas:

$$T_{W-ad} = z_{ad}/z_w \quad (15)$$

$$T_{C-ad} = A_{ad}/(F_{C-Ref}/m_c) \quad (16)$$

2.3.3. Predicting the effect of a rest support on system responses—The rest support is often connected to the grinding machine body (https://www.google.com/se, 1120); it is necessary to add a model of the machine body and a model of the rest support to the basic system model for the analyses. As the first degree of approximation for understanding the basic function of the support for vibration reduction, the machine body was crudely simulated as a set of mass-spring-damping elements (m_B, K_3, and C_3) added to the basic model, as shown in Fig. 3(a). While the actual machine body mass (m_B = 309.9 kg) was measured, the stiffness and damping values were estimated from the vibration spectra measured in the previous experimental study (Chen et al., 2017). It was found that the vibration peak at 40 Hz was substantially increased when a worn foot pad of the machine was replaced with a new one (Chen et al., 2017). This suggests that the fundamental resonant frequency of the machine installed on the floor at the workplace is likely to be close to or greater than 40 Hz. Then, $K_3 \geq 20{,}000$ kN/m. The measured body vibration spectra suggest that $C_3 \approx 10$ kN-s/m. A parametric study was also performed to explore the effects of the foot pad dynamic properties on the system responses by expressing the properties as functions of a proportional factor (Y) as follows:

$$K_3 = 2 \times 10^7 Y, \quad C_3 = 10^4 Y \tag{17}$$

Similarly, while it is difficult to determine K_2 and C_2 values, another parametric study was conducted to explore the effects of the drive wheel-body connection dynamic properties on the system responses by expressing them as functions of X in the simulations:

$$K_2 = 10^7 X, \quad C_2 = 8 \times 10^3 X \tag{18}$$

As shown in Fig. 1(a), the belt grinding machine simulated in this study is not equipped with any rest support. To help qualitatively understand the general effects of a rest support on the system responses, an additional set of elements (m_R, K_R, C_R, K_S, and C_S) representing a rest support was added to the system model, as also shown in Fig. 3(a). A series of parametric studies were performed to explore the variations of the rest support dynamic properties on the workpiece vibration by expressing the properties as functions of M, R, and S as follows:

$$m_R = M \tag{19}$$

$$K_R = RK_1 = 98682R, \quad C_R = RC_1 = 32.6R \tag{20}$$

$$K_S = SK_1 = 98682S, \quad C_S = SC_1 = 32.6S \tag{21}$$

Besides the machine vibration transmissibility and force-motion transmissibility calculated using Eqs. (2) and (3), the vibration transmissibility spectra on the machine body (T_{MB}) and rest support (T_{RS}) relative to the drive wheel were also calculated using the following formulas:

$$T_{MB} = z_B/z_w, \quad T_{RS} = z_R/z_w \tag{22}$$

The influence of the machine body vibration on the workpiece vibration can be eliminated by designing a rest support mounted directly on the ground (HSE, 2005), as shown in Fig. 3(b). This was crudely simulated using the additional model shown in Fig. 3(c). The dynamic properties for the rest support (m_R, K_R, C_R, K_S, and C_S) were also considered as variables in the analyses, the same as those expressed in Eq.(19)–(21).

3. Results

3.1. The basic responses of a handheld workpiece to machine vibration (F_W)

The machine vibration transmissibility of the handheld workpiece was predicted from Eq. (2) using the system responses yielded from Eq. (1) with $\boldsymbol{F}_W$ (F_W = 1.0) as the sole excitation and the model parameters listed in Table 1. The predicted transmissibility spectra for the six test treatments are illustrated in Fig. 4, together with their corresponding

experimental data measured in a previous study (Dong et al., 2018). The modeling results agree well with experimental data for each of the six test treatments in the major frequency range (20–1000 Hz) of concern. It should also be noted that the agreement was not imposed in the model calibration process, as the measured transmissibility spectra of the workpiece was not used in the model calibration (Dong et al., 2018). These observations suggest that the system model is valid for the prediction of the basic vibration response of the handheld workpiece.

3.2. The basic responses of a handheld workpiece to cutting vibration force (F_C) acting at the grinding interface

The force-motion transmissibility of the handheld workpiece was calculated from Eq. (3) using the modeling responses yielded from Eq. (1) with $\boldsymbol{F}_C$ ($F_C = 1.0$) as the sole excitation and the model parameters listed in Table 1. The calculated transmissibility spectra for the six test treatments are illustrated in Fig. 5. Different from the response to the machine vibration shown in Fig. 4, the response to the cutting vibration force is small for each test treatment in the low-frequency range (<25 Hz). This is because low-frequency vibration can be transmitted to the entire system; the interface vibration force must drive the mass of the entire system with fixed boundaries that restrict the system motion. With the reduction of the vibration transmission distance from its source, the response gradually increases with the increase in frequency before reaching a peak value for each test treatment. The peak value occurs at a frequency slightly higher than the undamped fundamental resonant frequency of the workpiece listed in Table 1, which was estimated from the workpiece mass (m_c) and the interface contact stiffness (K_1). Naturally, the increase in the interface contact stiffness shifts the resonance to a higher frequency range. There is a minor second peak in the force-motion transmissibility shown in Fig. 5. This peak is related to the major resonance of the fingers on the workpiece (Xu et al., 2018; Dong et al., 2018). At higher frequencies, the responses for all the test treatments decrease with the increase in frequency, but they all converge to its limit or unity (1.0), regardless of the grinding interface conditions. This is because the cutting vibration at high frequencies cannot be effectively transmitted beyond the workpiece; the resulting workpiece acceleration should become increasingly close to its free mass acceleration (F_C/m_c) with the increase in vibration frequency.

Fig. 6 shows direct comparisons of the two types of vibration transmissibility spectra (T_W and T_C) and their summations. Interestingly, the two types of transmissibility spectra are almost symmetrical with respect to the undamped resonant frequency of the workpiece at the interface. Both types of responses exhibit their large responses in the resonant frequency range. As a result, the summed response has a large peak in the resonant frequency range.

3.3. The workpiece vibration estimated from machine vibration

Fig. 7(a) illustrates the one-third octave band acceleration spectra of a large belt grinding machine (A_{MB}) reported in a previous study (Chen et al., 2017). They were measured on the machine body close to the grinding drive wheel operating at three different speeds (1,200, 1,800, 2400 rpm). The major peak frequency for each speed is associated with the operation speed of the drive wheel, which suggests that these peaks resulted primarily from the unbalanced mass of the drive wheel. Fig. 7(e) illustrates the reported vibration acceleration

spectra of handheld workpieces (golf club heads) ($A_{C\text{-}Measured}$) measured during their grinding on the same machine as that for the measurement of the machine body vibration (Chen et al., 2017). The peak frequencies at 20, 31.5, and 40 Hz for three speeds are the same as those observed in Fig. 7(a). There is also a common peak at about 125 Hz for each operating speed in both the machine body acceleration spectra (A_{MB}) and the measured workpiece acceleration spectra ($A_{C\text{-}Measured}$). However, their peak magnitudes are different. The overall trends of these two types of spectra are also different. As a result, the overall correlation between $A_{C\text{-}Measured}$ and A_{MB} in the frequency range of 20–125 Hz is not very good at some speeds, as shown in Fig. 8(a) and as reflected by the correlation coefficients listed in Table 2 (1st row of *R*-values). At higher frequencies (160–1600 Hz), the correlation between these two types of vibration spectra is poor for 1200 rpm and 1800 rpm but good for 2400 rpm, as indicated by the *R*-values also listed in Table 2.

The workpiece vibration spectrum resulting from the machine vibration at each speed was estimated from the machine body vibration shown in Fig. 7(a) using the approximate method described in Section 2.2. Each of the six pairs of the predicted T_W and T_C shown in Figs. 4 and 5 were tested in the estimations. Their corresponding *R*-values for each prediction stage in the two frequency ranges are listed in Table 2. As examples, Fig. 8 illustrates the regression curves of the correlations for Interface R55 under 30 N feed force and Fig. 7(b) illustrates the acceleration spectra ($A_{C\text{-}W}$) estimated using Eq. (5) with T_W for this test treatment, which represents the first part of the workpiece vibration resulting from the transmitted machine vibration in Eq. (8). The change of the regression slope (χ) does not affect the results of the correlation analyses, but its value ($\chi = 3$) was selected such that the estimated peak accelerations at 20, 30, and 40 Hz (related to the machine operation speeds) were comparable with those measured on the workpieces (Fig. 7(e)). As reflected by the *R*-values listed in Table 2 and the regression relationships shown in Fig. 8(a and b), the correlation between $A_{C\text{-}Measured}$ and $A_{C\text{-}W}$ for Interfaces R55 and R65 in the selected frequency range (20–125 Hz) is better than that between $A_{C\text{-}Measured}$ and A_{MB}. The improved correlation confirms that the machine vibration transmissibility (T_W) plays a certain role in determining the workpiece vibration. However, as also shown in Table 2, the correlation between $A_{C\text{-}Measured}$ and $A_{C\text{-}W}$ for Interface R45 generally became worse than that between $A_{C\text{-}Measured}$ and A_{MB}. This may be because R45 is a brand-new interface and its dynamic properties may not be sufficiently representative of those used in the measurement of the workpiece vibration in the reported study (Chen et al., 2017).

Fig. 7(c) illustrates the second part of the workpiece acceleration ($A_{C\text{-}CW}$) resulting from the transmitted machine vibration, which was estimated using Eq. (7) with T_W and T_C for Interface R55 under 30 N feed force. The transformation with T_C greatly improved the correlation ($A_{C\text{-}Measured}$ vs. $A_{C\text{-}CW}$) in the first frequency range (20–125 Hz) for every case, as shown in Table 2 and Fig. 8(c). In fact, a direct transformation with T_C alone ($T_C{*}A_{MB}$) also resulted in a very strong correlation for every case, as also shown in Table 2. This is because the T_C-transformation made the overall slope of the estimated spectra consistent with that of the measured workpiece vibration spectra in the selected frequency range. These observations confirm that the machine vibration can play a very important role in determining the cutting vibration force at the grinding interface (Oryński and Pawłowski, 1999; Hahn and Lindsay, 1970; Oliveira et al., 2008; Aurich et al., 2009), and that it

is essential to consider the force-motion transmissibility in the analysis of the workpiece vibration. However, as shown in Fig. 8(c), the T_C-transformation also skewed the correlation relationship: the data points in the low vibration range are all located at one side of the regression line for each case; the predicted vibrations at the frequencies (20, 31.5 and 40 Hz) related to the operation speeds shown in Fig. 7(c) are not comparable with the measured data shown in Fig. 7(e). This suggests that $A_{C\text{-}CW}$ alone is insufficient to fully represent the workpiece vibration resulting from the transmitted machine vibration, although the high R-values suggest that $A_{C\text{-}CW}$ is more important than $A_{C\text{-}W}$ in the cases examined in this study. Then, it is necessary to use Eq. (8) to estimate the total workpiece vibration resulting from the machine vibration.

The summed workpiece vibration ($A_{C\text{-}M}$) calculated using Eq. (8) for each operation speed is illustrated in Fig. 7(d). The constant (ζ/m_c) in Eq. (8) actually represents the relative weighting of the interface cutting vibration ($A_{C\text{-}CW}$) resulting from the machine vibration in its combination with the directly-transmitted machine vibration ($A_{C\text{-}W}$). Because $A_{C\text{-}CW}$ is more important than ($A_{C\text{-}W}$), $A_{C\text{-}CW}$ should have larger weighting in the combination to form the estimated final workpiece vibration. Therefore, The constant ($\zeta/m_c = 2.5$) was determined such that the $A_{C\text{-}M}$ spectra shown in Fig. 7(d) for all the three operation speeds were comparable with those measured on the workpieces (Fig. 7(e)), while the correlations between $A_{C\text{-}M}$ and $A_{C\text{-}Measured}$ spectra in the selected frequency range remained at a high level (Table 2). As shown in Fig. 8(d), the regression relationship for the correlation between $A_{C\text{-}W}$ and $A_{C\text{-}Measured}$ at each operation speed is much less skewed than that shown in Fig. 8(c).

3.4. The effects of intervention methods on workpiece response functions

As found in exploring analyses, the use of different sets of interface stiffness (K_1) and damping (C_1) values listed in Table 1 in the described analyses do not change the basic trends of the effects of intervention methods on workpiece response functions. As examples, the modeling results of the intervention methods obtained with the K_1 and C_1 values listed in Table 1 for Interface R55 under a 30 N feed force as the basis in the analyzes were presented in this section. The T_w and T_C spectra calculated with the K_1 and C_1 values from the original model shown in Fig. 1(c) were used as the baseline references for the comparisons to clearly identify the potential effects of each analyzed intervention method.

3.5. The effects of the interface dynamic properties on workpiece responses

As shown in Fig. 9, proportionally reducing the interface stiffness and damping values can generally reduce the fundamental resonant frequency of the workpiece on the grinding interface and its vibration in the entire frequency range of concern.

3.6. The effects of workpiece adapters on workpiece responses

As shown in Fig. 10(a), adding a solid adapter or mass to the workpiece without changing the grinding interface conditions or feed force can reduce the fundamental resonant frequency of the workpiece. The added mass can also proportionally reduce the force-motion transmissibility in the frequency range above the resulting resonant frequency of the

workpiece, as shown in Fig. 10(b). However, results shown in Fig. 10(a) also indicate that the added mass can substantially increase the major resonant peak.

As shown in Fig. 11, in addition to the solid adapter, installing a vibration absorber on the adapter can further reduce the workpiece vibration in the original resonant frequency range. Its effectiveness, however, depends on the combination of the mass, stiffness, and damping values of the vibration absorber.

As predicted with the model shown in Fig. 2(b), if some cushioning materials are inserted between an adapter and the workpiece, and the adapter is held by the hands of a grinding operator, the vibration on the adapter at frequencies above the fundamental resonant frequency of the workpiece can be substantially reduced, especially in the very high*frequency range, as shown in Fig. 12. This is because the cushioning function generally increases with the increase in vibration frequency. The effectiveness of this intervention method also increases with the reduction of the cushion stiffness. This cushioning method, however, may increase the adapter vibration at frequencies below the original resonant frequency of the workpiece, as also shown in Fig. 12.

3.7. The effects of rest supports on workpiece responses

If a rest support is connected to the machine body, as simulated in the model shown in Fig. 3(a), the workpiece vibration in the original resonant frequency range can be substantially reduced, as shown in Fig. 13. However, the workpiece vibration at some lower frequencies may be largely increased, depending on the dynamic properties of the machine body and rest support, as also shown in Fig. 13.

Fig. 14 illustrates direct comparisons of the vibration transmissibility spectra of the machine body, rest support, and workpiece for four different sets of machine connection properties. Obviously, the new resonant peak frequency of the workpiece on the rest support is approximately the same as that of the machine body and rest support. Both the machine body and rest support resonances can significantly affect the workpiece response peak frequency and magnitude.

Fig. 15 illustrates the effects of an independent rest support on the workpiece responses. The physical separation of the rest support from the machine body had little influence on the force-motion transmissibility if the dynamic properties of the rest support remain unchanged, as shown in the right columns of Figs. 13 and 15. However, the separation greatly reduced the machine vibration transmissibility of the workpiece, as shown in the left columns of Figs. 13 and 15. Increasing the stiffness, damping, and effective mass values of the independent rest support further reduced the machine vibration transmissibility, as shown in Fig. 15(c1).

4. Discussion

Although a specific set of model parameters were used in the analyses, the proposed methodology for the analyses and the findings on the basic characteristics of the workpiece vibration responses, the general effectiveness of various engineering intervention methods,

and the basic influences of intervention system properties should be generally applicable. They, together with their implications, are further elaborated and discussed in this section.

4.1. General implications of the workpiece response functions

The characteristics of the two response functions shown in Figs. 4–6 theoretically prove that the workpiece vibrations in the low- and low/middle-frequency ranges on many belt grinding machines are likely to be associated primarily with the grinding machine vibration. This is further confirmed by the combined modeling and experimental results illustrated in Fig. 7. The current standard method for assessing the risk of hand-transmitted vibration exposures emphasizes this frequency range (ISO 5349–1, 2001). Therefore, the control of the machine vibration should be at the top of the list of strategies for minimizing grinding operator hand-transmitted vibration exposures. This can be achieved by selecting or developing low-vibration grinding machines, regularly monitoring the machine vibration, and maintaining the machines in good condition. Some standards and technologies have been established or developed to help achieve these objectives (ISO ISO 20816–1, 2016; ISO 21940–1, 2019). Alternatively, reducing the stiffness of grinding interface and/or using a solid seat support can also effectively reduce the workpiece vibration in the low and middle frequency ranges, as shown in Figs. 9 and 15.

As shown in Fig. 6, both types of vibration sources can result in large workpiece responses in the resonant frequency range. The resonant responses can be attenuated by using a workpiece adapter equipped with a vibration absorber, as shown in Fig. 11. The useful frequency range of the adapter can be effectively extended by using the nonlinear technique reported in a recent study (Lindell et al., 2015). The use of a seat support can also effectively reduce the resonant responses, as shown in Fig. 15.

At higher frequencies, the force-motion transmissibility (T_C) plays the dominant role in determining the overall response, as also shown in Fig. 6. Several studies found that high-frequency vibration exposures to fingers could also be harmful (Starck et al., 1990; Dandanell and Engstrom, 1986). It is always desired to reduce the exposure as much as feasible. Because some high-frequency cutting forces may be useful to maintain the grinding quality and efficiency (Tönshoff and Degenhardt, 1982; Oryński and Pawłowski, 1999; Hahn and Lindsay, 1970; Oliveira et al., 2008; Aurich et al., 2009), it is neither desired nor feasible to eliminate them in the workpiece grinding process. Fortunately, while it is difficult to find or develop a practically useable vibration-reducing (VR) glove to effectively reduce the low-frequency vibrations transmitted to the fingers, VR gloves can effectively attenuate high-frequency vibrations and reduce sharp peaks, especially for vibration frequencies above 1000 Hz (Welcome et al., 2012; Xu et al., 2019). As shown in Figs. 10–12, some intervention methods can also be used to effectively reduce the vibrations that could result from high-frequency cutting forces without affecting the grinding efficiency.

As anticipated, there are some differences between the estimated workpiece responses and the measured vibration data, especially at frequencies higher than 125 Hz, as shown in Fig. 7. They result from the following reasons/sources:

- The actual transfer function between the drive wheel and machine body was not available because it is extremely difficult to reliably measure the vibrations on the rotating drive wheel. As the first degree of approximation, a linear transformation was actually used to represent the transfer function, as expressed in Eq. (4). This is reasonable in the low- and middle-frequency ranges, because the connection between the drive wheel and the machine body must be stiff. This, however, can introduce a large error in the estimated high-frequency vibrations.
- The linear transformation from the input vibration motion to the vibration force expressed in Eq. (6) is also a first-degree approximation, as the real transfer function could be very complicated.
- The excitations stemming from the geometric and material irregularities at the grinding interface were not considered in the estimation. This is unlikely to change the basic trends of the estimated response spectrum below the fundamental resonant frequency of the workpiece (about 125 Hz) because the excitations on the belt grinding interface are primarily observed in the high-frequency range (Tönshoff and Degenhardt, 1982), and the T_C value in the low-frequency range is much less than the T_W value, as shown in Fig. 6. This, however, is not the case at higher frequencies.

For these reasons, the method expressed in Eq. (8) can only be used to estimate the workpiece vibrations below the fundamental resonant frequency of the workpiece and resulted from the vibrations measured at a point on the machine body close to the drive wheel. Furthermore, the regression coefficients ($\chi = 3$, $\zeta = 2.5m_c$) could also vary with different machines and workpieces. However, these limitations or deficiencies do not affect the validity of the methodology proposed and used in this study to evaluate the effectiveness of the engineering control methods based on the two transfer functions (T_W, T_C); the crude estimation method was only designed and used to test the hypothesis on the two vibration transmission pathways from the drive wheel to the workpiece and to demonstrate that the two transfer functions (T_W, T_C) play an essential role in determining the workpiece vibrations.

4.2. Reducing the workpiece vibration by changing the grinding interface dynamic properties

The modeling results illustrated in Fig. 9 suggest that the workpiece vibration in the entire frequency range of concern generally decreases with the reduction of the grinding interface hardness if the other grinding conditions remain unchanged. These results suggest that reducing the feed force, and especially the material stiffness, can reduce the vibration exposure. As shown in Fig. 4, the use of interface R45 (a brand-new wheel rubber tread) is obviously better than the other two interfaces (R55 and R65 were used and partially worn). This suggests that the wheel rubber tread should be replaced with a new one when it is worn to a certain extent.

The results shown in Figs. 5 and 9 also suggest that this intervention method is especially effective in the original resonant frequency range and at higher frequencies, but it may not

be effective at the heavily-weighted lower frequencies. However, the interface hardness must be substantially reduced (e.g., >50% of the reference value (K_1 = 96.828 kN/m)). It may be difficult to further reduce the interface stiffness by simply replacing the rubber tread on the belt grinding machine with a much softer rubber tread; such a replacement may increase not only the machine noise but also the unbalanced mass of the drive wheel which may result in higher machine vibrations (Tönshoff and Degenhardt, 1982). A grinding machine designed to operate a flexible grinding disc may be selected to realize a substantial reduction in the grinding interface hardness (https://www.google.com/se, 1120). Alternatively, a free belt grinding machine can also be considered (https://www.google.com/se, 1120). Unfortunately, the reduction of the interface stiffness is likely to reduce the grinding efficiency or productivity (Tönshoff and Degenhardt, 1982). In addition to other factors (e.g., the geometric requirement of the ground surfaces and the desired surface quality), the grinding machine with a soft interface is usually selected to conduct the final fine grinding or polishing of workpiece surfaces. Then, the workpiece vibration in a polishing process should be generally less than that in the other grinding processes. This theoretical prediction is consistent with field observation (Chen et al., 2017).

4.3. The effects of workpiece mass on its vibration

The modeling responses illustrated in Fig. 10 suggest that increasing the mass of a workpiece may reduce the vibration exposure in the high-frequency range, but such a change may reduce or increase the vibration resulting from the machine vibration, primarily depending on the dominant frequency range of the machine vibration. For example, because the dominant weighted machine vibrations shown in Fig. 7(a) are in the range of 20–40 Hz, increasing the workpiece mass should increase the frequency-weighted acceleration of the workpiece. This is consistent with that observed in the previous study (Chen et al., 2017): the ground steel alloy golf club heads weighed more than the ground titanium club heads; the weighted acceleration of the alloy club heads for every machine operating speed on each model of grinding machines (large and small) was larger than that of the titanium club heads. However, it should be noted that the change of workpiece mass is usually accompanied with the changes of workpiece material, grinding surface geometries, hand coupling conditions, etc.; these changes may also influence the workpiece vibration. As a result, it may not be reliable to predict the workpiece vibration solely based on the weight or mass of a workpiece.

4.4. The effectiveness and limitations of adapter methods

As above-mentioned, a set of locking pliers or a handle may be firmly attached to a small workpiece to help safely conduct the workpiece grinding (https://www.familyhandyma, 2020; https://www.youtube.com/w, 2020). Some special adapters may also be designed to achieve the same purpose. Their effects on the workpiece vibration responses are the same as if the workpiece mass is substantially increased. As above-discussed, these adapter methods are unlikely to be effective in the low/middle-frequency range, but these techniques should be very effective for reducing high-frequency vibration exposures. Furthermore, the use of these adapter methods has the following potential ergonomic benefits: (i) the adapter can be designed to change the finger pinch grip on a workpiece to a power grip on the adapter, which can increase the skin contact surface area, reduce hand and arm

muscle forces, and minimize their fatigue; and (ii) if the adapter/workpiece is suspended or supported, there may be a further reduction in the required grip force to perform the task. The suspension system or adapter support may also reduce vibration transmission; these potential benefits are further discussed in the following paragraphs and in section 4.5.

As illustrated in Fig. 11, the workpiece vibration can be further reduced in the original resonant frequency range if a vibration absorber is added to the adapter. Compared with the simple adapter method also shown in this figure ($\eta = +\infty$ *or* $m_{ad} = 200$ g), the added vibration absorber can also significantly expand the effective frequency range of the adapter. This intervention method may be useful to reduce the workpiece vibration in the major resonant frequency range, for example, the vibration peaks in the range of 80–160 Hz shown in Fig. 7(e). A unique feature of the vibration absorber method is that it can be designed to effectively target the vibration peak at a specific frequency. For example, as shown in Fig. 11(a), the vibration at 80 Hz can be greatly reduced (>50%) using an adapter/absorber with $\eta = 0.25$ or with an absorber alone ($m_{ad} = 0$) but with $m_{ab} = 200$ g and $\eta = 0.5$. If the workpiece has a hollow space, simply filling the space with sand or clay may substantially reduce the vibrations in the resonant frequency range and at higher frequencies, as the added sand or clay is likely to function similarly to a vibration absorber.

The suspended adapter method is better than the simple mass adapter method, especially in the high-frequency range, as shown in Fig. 12. However, similar to the other adapter methods, it may amplify the vibration at frequencies below the original resonant frequency. To extend the effective frequency range to below 20 Hz, the suspension stiffness must be greatly reduced. This may make it impossible for the operator to safely and effectively control the workpiece during grinding. Alternatively, the adapter mass can be greatly increased to extend the effective frequency range. This, however, may substantially increase the burden of the hand-arm systems and can reduce productivity. A suspension system or mechanical arm may be used to support the adapter and/or workpiece, similar to that used to support a handheld grinder (McDowell et al., 2016). Then, the intervention becomes similar to the rest support method discussed in the next section.

4.5. The effectiveness and limitations of rest support methods

As illustrated in Figs. 13 and 15, a rest support can greatly reduce the workpiece vibration in the original resonant frequency range, and this method is generally more effective than any of the other investigated intervention methods. However, these support systems may not reduce much workpiece vibration at very high frequencies, as shown in the right columns of these figures. Fortunately, as above-discussed, the very high-frequency vibration can be effectively attenuated using other methods.

The results shown in Fig. 14 indicate that the machine body vibration can significantly affect the vibration on the rest support connected to the machine body, and that the machine body resonance, rest support resonance, or both could result in high workpiece vibration. The physical separation of the rest support from the machine body can effectively reduce the workpiece vibration in the low- and middle-frequency range, especially when the rest support has a rigid structure and is firmly mounted on the ground, as shown in Fig. 15(c1). These modeling predictions are consistent with those observed at workplaces (HSE, 2005).

These modeling predictions further suggest that if feasible and practical, the rest support should not be connected to the machine body, but it should have a rigid structure and be firmly mounted to the floor, especially for machines extensively used to perform grinding daily.

Theoretically, a metal to metal contact has the largest contact stiffness and promotes the highest rest support effectiveness. Practically, however, this may not be the best choice if the workpiece has a contact resonance on the metal surface of the rest surface with little damping. Such a resonance was observed in our experimental study during the measurement of the impedance of the workpiece-hand-arm system on a stiff interface (Xu et al., 2018). The modeling results shown in Fig. 15 suggest that it is not necessary to maintain the metal-to-metal contact to maximize the effectiveness of the rest support. We hypothesize that attaching a thin layer of non-metal material such as rubber on the rest support surface may avoid any sharp resonance on the rest support while maintaining the benefits of the rest support. This hypothesis should be tested in further studies.

5. Conclusions

This study created a methodology based on a model of a belt grinding machine-workpiece-hand-arm system for characterizing the workpiece vibration responses to two types of excitations (machine vibration and interface excitation) and for evaluating various engineering control methods associated with the vibration transmissions in the system. This study enhanced the understanding of the handheld workpiece vibration in the following aspects:

I. While the conventional vibration transfer function can be used to characterize the workpiece response to machine vibration, a new transfer function termed as ‘force-motion transmissibility’ defined in this study can be used to characterize the workpiece response to interface excitation. These two types of transfer functions are almost symmetrical with respect to the fundamental resonant frequency of the workpiece in the system. This characteristic indicates that while the workpiece vibration generally depends on both types of excitations, the workpiece vibration in the low-frequency range depends primarily on the machine vibration. However, the workpiece vibration depends primarily on interface excitation at very high frequencies. Both types of transfer functions can play an important role in modeling the workpiece vibration in its resonant frequency range. An effective method to shift the workpiece resonant frequency is to change the grinding interface stiffness.

II. The results of this study confirm that the machine vibration transmitted to the grinding interface can not only be directly transmitted to the workpiece, but it can also serve as an important interface excitation resulting in the workpiece vibration. Therefore, there are generally two mechanisms or pathways that influence the workpiece vibration resulting from the machine vibration: (1) the direct transmission that depends on the machine vibration transmissibility; and (2) the indirect transmission that depends on both the machine vibration

transmissibility and the force-motion transmissibility. Both mechanisms should be considered in the estimation and understanding of workpiece vibrations.

This study applied the proposed methodology to analyze several engineering methods for controlling workpiece vibrations. The analyses clarified the basic mechanisms of these vibration control methods and explored their potential effectiveness, features, and limitations. The results of modeling analyses suggest that some combinations of intervention methods can minimize workpiece vibration exposures without reducing the grinding efficiency or productivity. For example, while the vibration in low- and middle-frequency range can be most effectively controlled by designing a special independent rest support for each grinding machine, high-frequency vibrations can be effectively minimized by developing an anti-vibration adapter for the grinding of workpiece surfaces, in addition to the use of vibration-reducing gloves. While the modeling methodology developed in this study can be used to explore and analyze more intervention methods for controlling workpiece vibrations, the presented modeling results and discussions can be used to guide the selection of appropriate vibration control methods and to help design vibration-reducing devices for controlling the vibration exposures of workers performing handheld workpiece grinding.

References

Aurich JC, Biermann D, Blum H, Brecher C, Carstensen C, Denkena B, Klocke F, Kröger M, Steinmann P, Weinert K, 2009. Modelling and simulation of process: machine interaction in grinding. J. Inst. Eng. Prod3 (1), 111–120.

Chen QS, Xiao B, Yang AC, Lin HS, Yan H, Lang L, Yan MS, Chen GP, Zeng FS, Cao XQ, 2015. The characteristics of vibration-induced white finger in workers polishing handheld pieces in the southern subtropics of China. In: The Proceedings of the 13th International Conference on Hand-Arm Vibration, pp. 19–20. Beijing, China.

Chen Q, Lin H, Xiao B, Welcome DE, Lee J, Chen G, Tang S, Zhang D, Xu G, Yan M, Yan H, Xu XS, Qu H, Dong RG, 2017. Vibration characteristics of golf club heads in their handheld grinding process and potential approaches for reducing the vibration exposure. Int. J. Ind. Ergon62, 27–41. [PubMed: 30514986]

Dandanell R, Engstrom K, 1986. Vibration from riveting tools in the frequency range 6 Hz-10 MHz and Raynaud's phenomenon. Scand. J. Work. Environ. Health12, 338–342. [PubMed: 3775319]

Dong RG, Lin H, Xiao B, Welcome DE, Lee J, Chen G, Tang S, Zhang D, Xu G, Yan M, Yan H, Xu XS, Qu H, Chen Q, 2016. Potential approaches for reduction the vibration exposure of workers performing handheld grinding of golf club heads. In: Proceedings of the 6th American Conference on Human Vibration. Medical College of Wisconsin and Marquette University, Milwaukee, WI, USA, pp. 29–30.

Dong RG, Welcome DE, Xu XS, Chen Q, Lin H, McDowell TW, Wu JZ, 2018. A model for simulating vibration responses of grinding machine-workpiece-handarm system. J. Sound Vib431, 276–294.

Griffin MJ, 1990. Handbook of Human Vibration. Academic Press, London.

Hahn RS, Lindsay RP, 1970. The influence of process variables on material removal, surface integrity, surface finish and vibration in grinding. In: Advances in Machine Tool Design and Research - Proceedings of the 10th International M.T.D.R. Conference, pp. 95–117.

HSE, 2005. Hand-Arm Vibration the Control of Hand-Arm Vibration 2005 Guidance on Regulations. HSE Books, UK.

https://www.familyhandyman.com/tools/power-tools/bench-grinder-basics/. (Accessed 19 February 2020).

https://www.google.com/search?q=belt+grinding+machine+vibration&tbm=isch&source=univ&safe=strict&sa=X&ved=2ahUKEwi02YPgy9XjAhXOneAKHY7PD8wQsAR6BAgDEAE&biw=1120&bih=587. (Accessed 19 February 2020).

https://www.youtube.com/watch?v=ZLfgjeq86fw. (Accessed 19 February 2020).

Ikeda K, Ishizuka H, Sawada A, Urushiyama K, 1998. Vibration acceleration magnitudes of hand-held tools and workpieces. Ind. Health36, 197–208. [PubMed: 9583318]

ISO5349–1, 2001. Mechanical Vibration — Measurement and Evaluation of Human Exposure to Hand-Transmitted Vibration — Part 1: General Requirements. International Organization for Standardization, Geneva, Switzerland.

ISO21940–1, 2019. Mechanical Vibration – Rotor Balancing – Part 1: Introduction. International Organization for Standardization, Geneva, Switzerland.

Kaulbars U, 2014. Hand-arm vibration – risk assessment in dental laboratories. In: The Proceedings of the 22nd Japan Conference on Human Response to Vibration, pp. 5–14. Okinawa, Japan.

Lindell H, Berbyuk V, Gretarsson SL, Josefsson M, 2015. Hand-held impact machines with nonlinearly-tuned vibration absorber. In: The Proceedings of the 13th International Conference on Hand-Arm Vibration (Beijing, China).

McDowell TW, Welcome DE, Warren C, Xu XS, Dong RG, 2016. The effect of a mechanical arm system on portable grinder vibration emissions. Ann. Occup. Hyg60 (3), 371–386. [PubMed: 26628522]

ISO20816–1, 2016. Mechanical Vibration – Measurement and Evaluation of Machine Vibration – Part 1: General Guidelines. International Organization for Standardization, Geneva, Switzerland.

Oliveira JFG, França TV, Wang JP, 2008. Experimental analysis of wheel/workpiece dynamic interactions in grinding. CIRP Ann. 57, 329–332.

Oryński F, Pawłowski W, 1999. The influence of grinding process on forced vibration damping in headstock of grinding wheel of cylindrical grinder. Int. J. Mach. Tool Manufact39 (2), 229–235.

Starck J, Jussi P, Ilmari P, 1990. Physical characteristics of vibration in relation to vibration-induced white finger. Am. Ind. Hyg. Assoc. J51 (4), 179–184. [PubMed: 2327329]

Tönshoff HK, Degenhardt H, 1982. Noise and vibration in belt grinding at contact wheels. CIRP Ann. - Manuf. Technol31 (1), 281–286.

Welcome DE, Dong RG, Xu XS, Warren C, McDowell TW, 2012. An evaluation of the proposed revision of the anti-vibration glove test method defined in ISO-10819 (1996). Int. J. Ind. Ergon42 (1), 143–155.

Xu XS, Welcome DE, Warren CM, McDowell TW, Lin H, Xiao B, Chen Q, Dong RG, 2018. The vibration responses of a handheld workpiece and the hand arm system. In: Proceedings of the 7th American Conference on Human Vibration. University of Washington, Department of Environmental and Occupational Health Sciences, Seattle, WA, USA, pp. 88–89.

Xu XS, Welcome DE, Warren C, McDowell TW, Dong RG, 2019. Development of a finger adapter method for the test and evaluation of vibration-reducing gloves and materials at fingers. Measurement137, 362–374. [PubMed: 30948862]

Relevance to the industry

Significant prevalence of hand-arm vibration syndrome has been found among workers performing the grinding of handheld workpieces in recent years. How to effectively control their vibration exposures remains an important issue. This study analyzed and explored various engineering intervention methods and identified effective control methods. The findings can be used to help select appropriate intervention methods and to guide the development of more effective control technologies.

(a) A grinding operation

(b) Vibration sources and transmission pathways

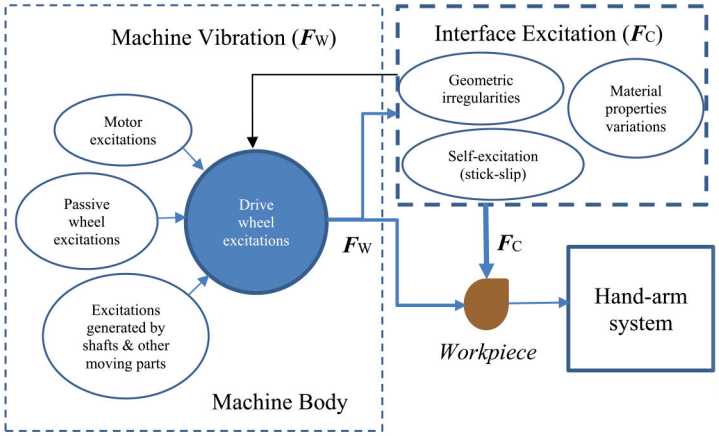

(c) Basic system model

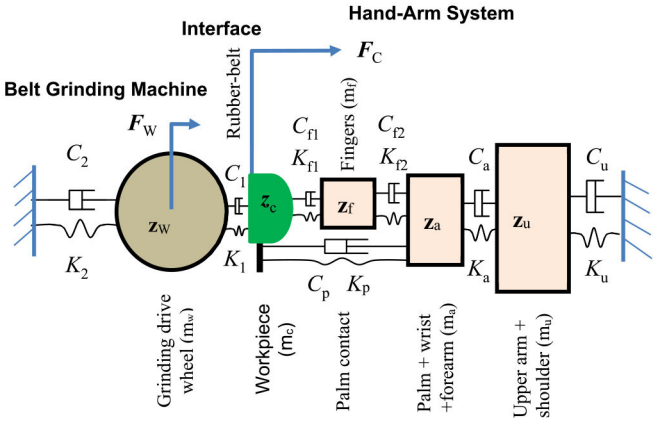

Fig. 1.

The simulation of a grinding operation on a belt grinding machine: (a) a pictorial view of the grinding of a workpiece held by two hands of a worker (Chen et al., 2017); (b) vibration sources and transmission flowchart, in which F_W represents the overall equivalent machine vibration force acting on the grinding drive wheel of the machine, and F_C represents the overall equivalent cutting vibration force acting on the workpiece; and (c) a model of the grinding machine-workpiece-hand-arm system (Dong et al., 2018), in which **z** represents the displacement of each lumped mass in the system, K represents connecting stiffness in the system, and C represents its damping values.

(a) Adapter with a vibration absorber (b) Suspended adapter held by the hands

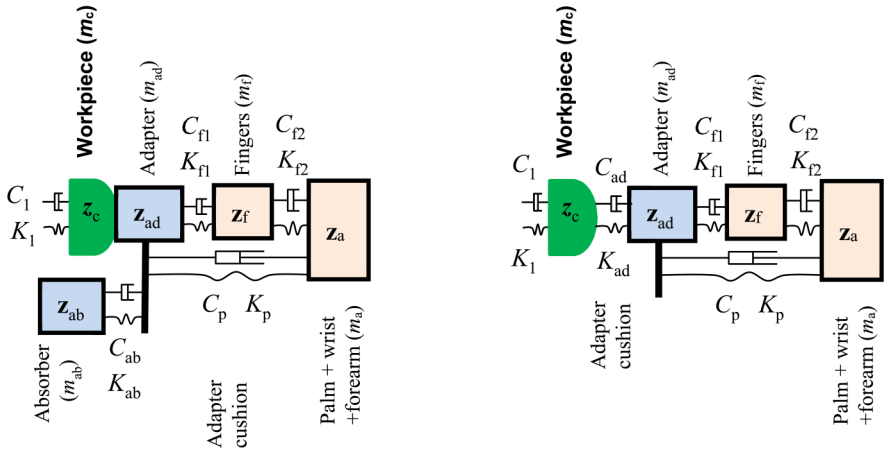

Fig. 2.

A portion of the system model with added adapters: (a) the adapter (m_{ad}) with a vibration absorber (m_{ab}, K_{ab}, C_{ab}) held by the hands; (b) suspended adapter (m_{ad}) held by the hands and with some cushioning (K_{ad}, C_{ad}) between the workpiece and the adapter.

(a) The system model with a rest support connected to the machine body

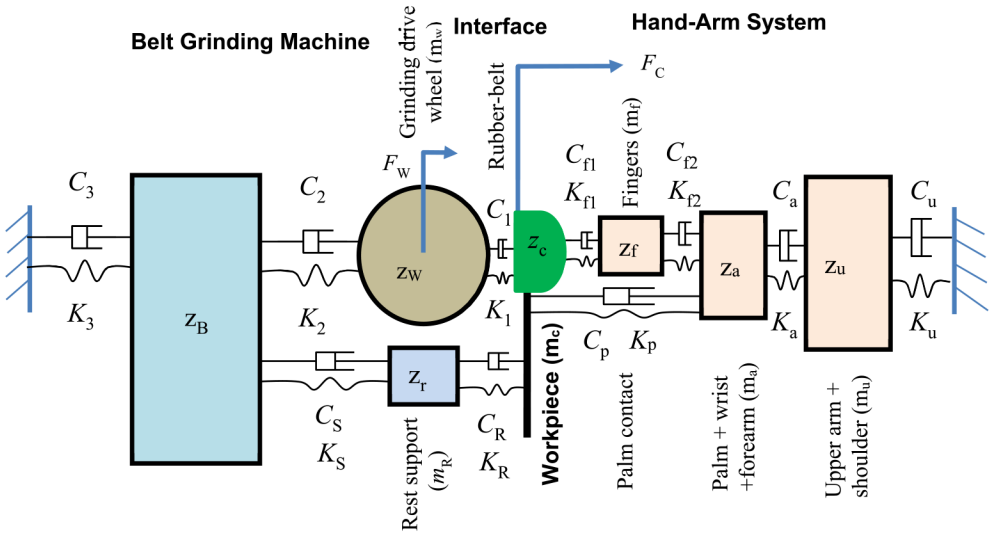

(b) Machine with an independent rest support

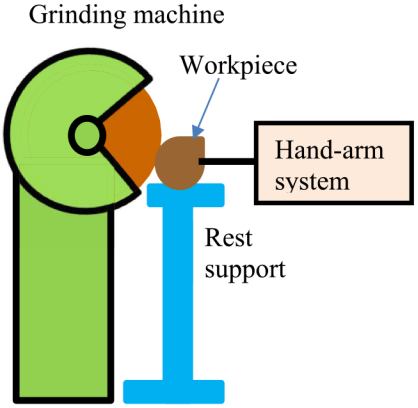

(c) Part of the model with independent rest support

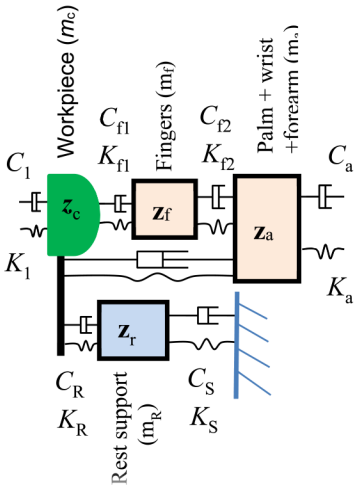

Fig. 3.

The simulation of the grinding of a workpiece in contact with a rest support: (a) the system model with a rest support connected to the body of the grinding machine; (b) the sketch of a grinding machine equipped with an independent support; (c) a portion of the system model with an independent rest support.

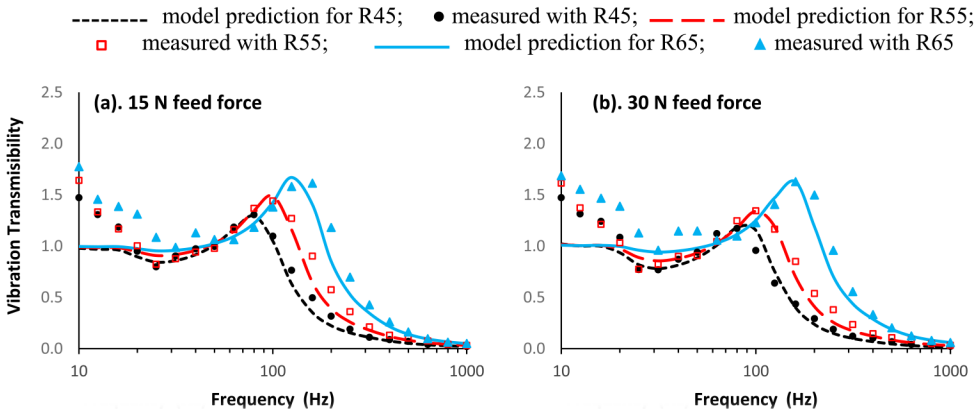

Fig. 4.

Comparisons of the predicted and measured vibration transmissibility spectra of a handheld workpiece subjected to the excitation from the grinding machine or drive wheel (F_W) under two feed forces on three grinding interfaces (R45, R55, and R65): (a) 15 N feed force; (b) 30 N feed force.

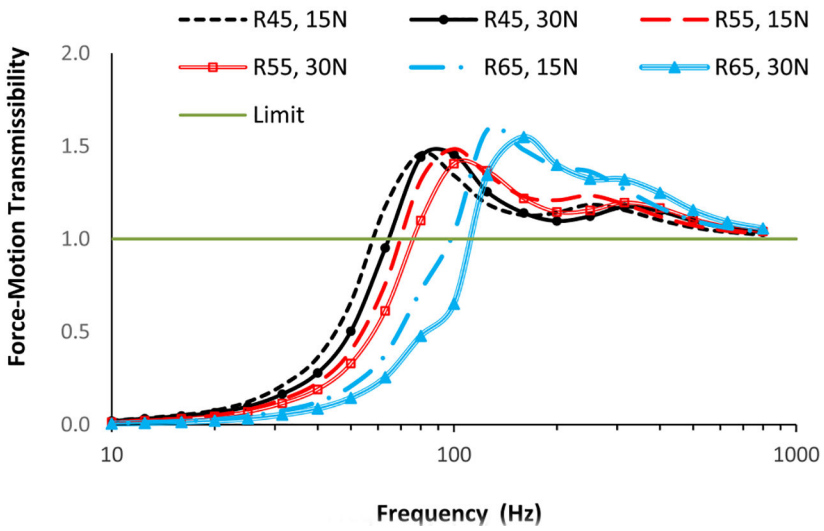

Fig. 5.

The modeling responses of a handheld workpiece subjected to the excitation force from the grinding contact interface (F_C) under two feed forces (15 N and 30 N) on three grinding interfaces (R45, R55, and R65).

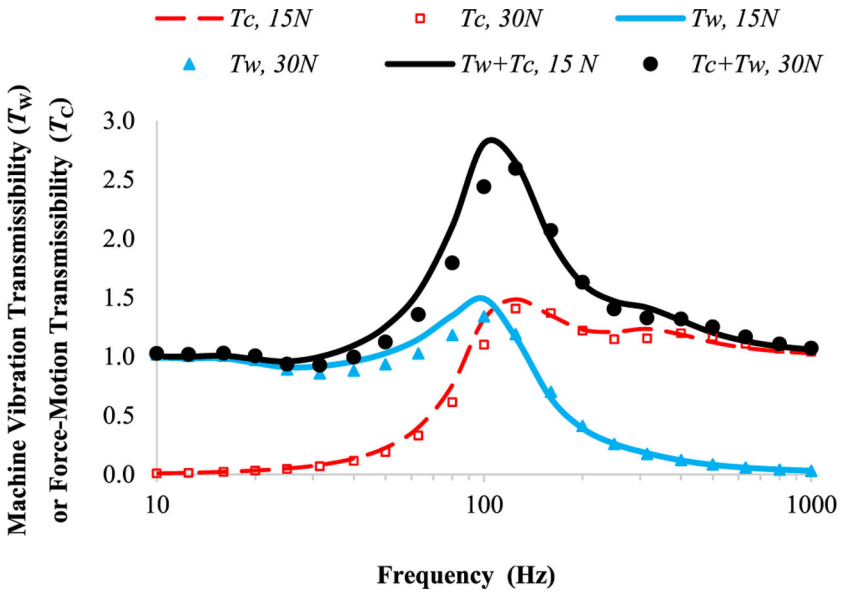

Fig. 6.

Comparisons of the two types of vibration transmissibility spectra (T_W and T_C) on the interface R55.

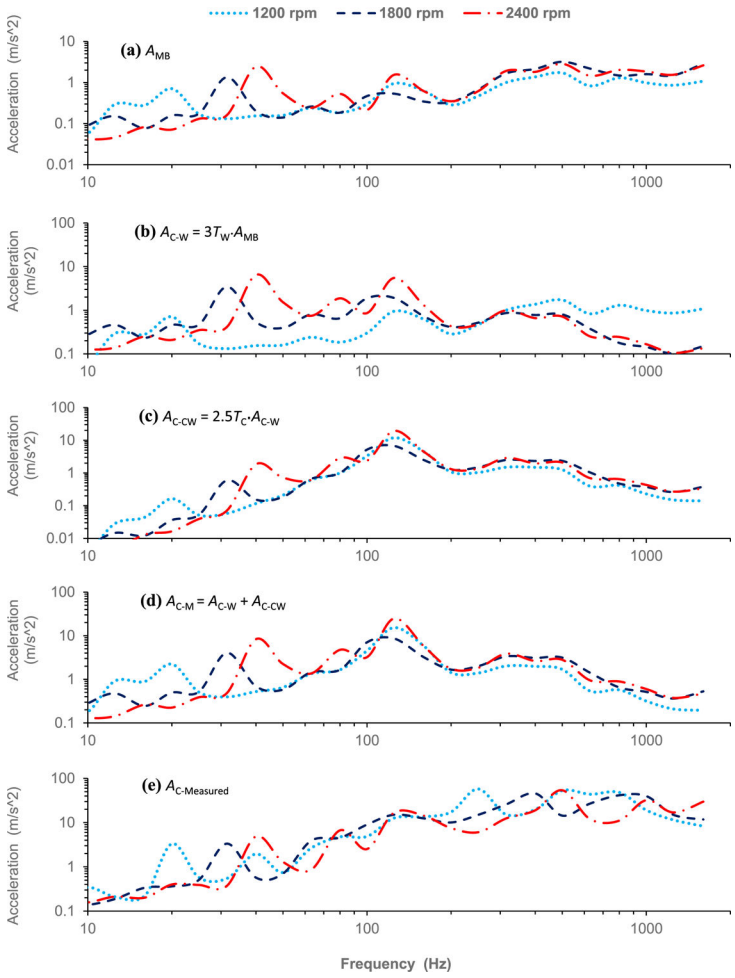

Fig. 7.

Comparisons of the measured acceleration spectra at three different operation speeds with those estimated using T_W and T_C for R55 interface under 30 N feed force: (a) the measured machine body acceleration (A_{MB}) (Chen et al., 2017); (b) the estimated acceleration transmitted from the machine to the workpiece ($A_{C\text{-}W} = \chi * T_W * A_{MB}$, in which $\chi = 3$); (c) the acceleration induced from the machine-transmitted vibration ($A_{C\text{-}CW} = T_C * A_{C\text{-}W} * \zeta/m_c$, in which $\zeta/m_c = 2.5$); (d) the model-estimated workpiece acceleration ($A_{C\text{-}M} = A_{C\text{-}W} + A_{C\text{-}CW}$); (e). The measured workpiece acceleration ($A_{C\text{-}Measured}$) (Chen et al., 2017).

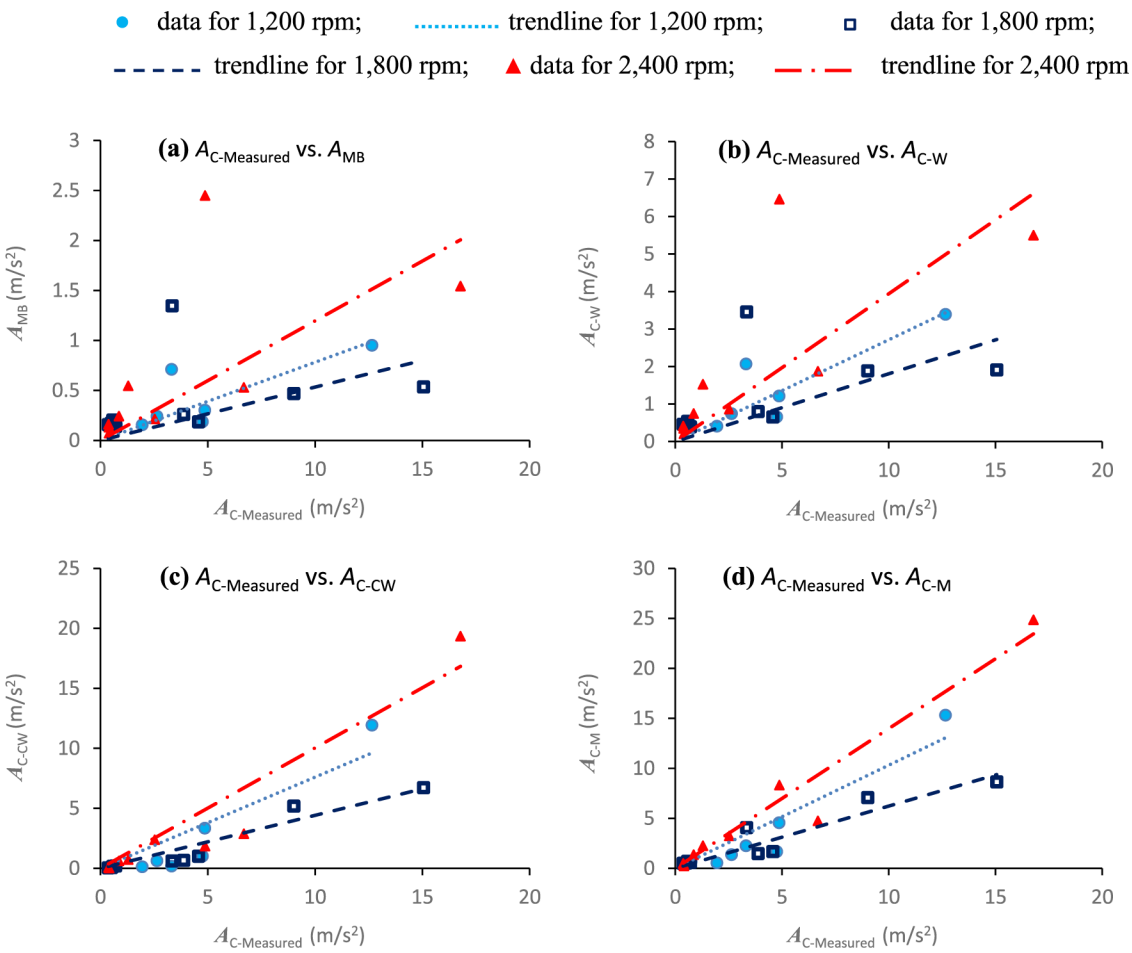

Fig. 8.

The correlations in the frequency range of 20–125 Hz between the measured workpiece vibrations ($A_{C\text{-}Measured}$) for three different machine operating speeds and their corresponding vibrations estimated using T_W and T_C for R55 interface under a 30 N feed force: (a) $A_{C\text{-}Measured}$ vs. machine body vibration (A_{MB}); (b) $A_{C\text{-}Measured}$ vs. the estimated vibration transmitted from the machine to the workpiece ($A_{C\text{-}W} = \chi * T_W * A_{MB}$, in which $\chi = 3$); (c) $A_{C\text{-}Measured}$ vs. the vibration induced from the machine-transmitted vibration ($A_{C\text{-}CW} = T_C * A_{C\text{-}W} * \zeta/m_c$, in which $\zeta/m_c = 2.5$); (d) $A_{C\text{-}Measured}$ vs. the estimated workpiece vibration ($A_{C\text{-}M} = A_{C\text{-}W} + A_{C\text{-}CW}$).

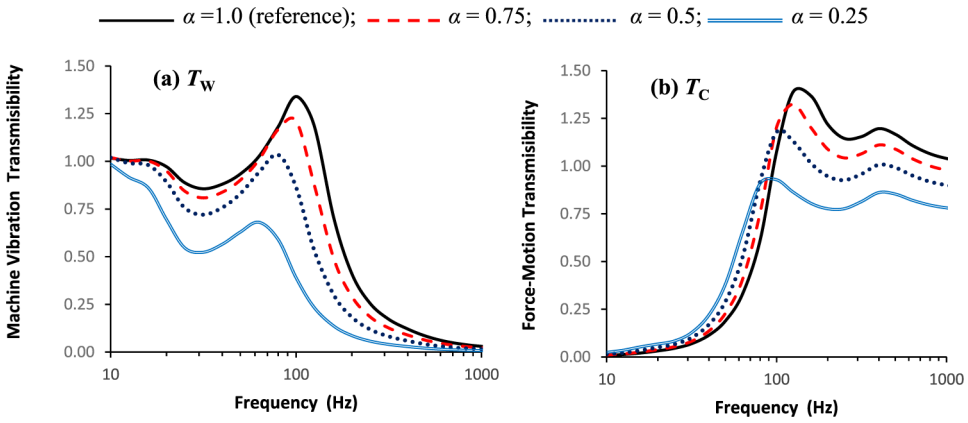

Fig. 9.

The effects of interface dynamic properties on workpiece vibration: (a) machine vibration transmissibility; (b). force-motion transmissibility with $\beta = 0.2$.

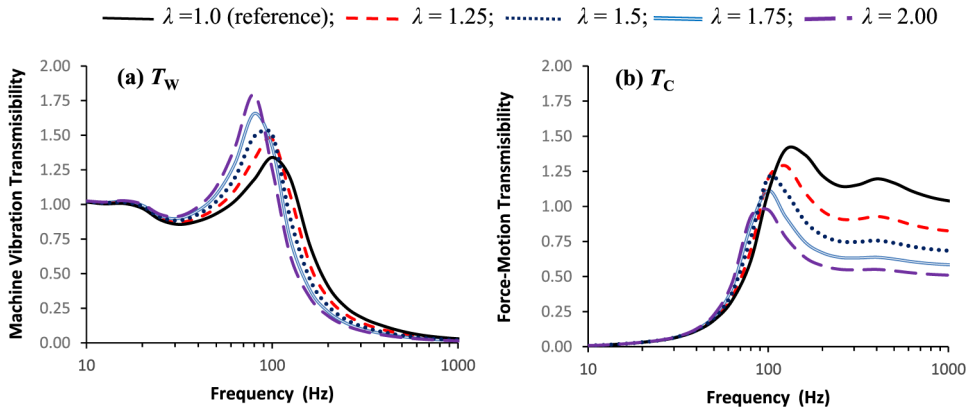

Fig. 10.

The effects of adapter mass on workpiece vibration: (a) machine vibration transmissibility; (b) force-motion transmissibility.

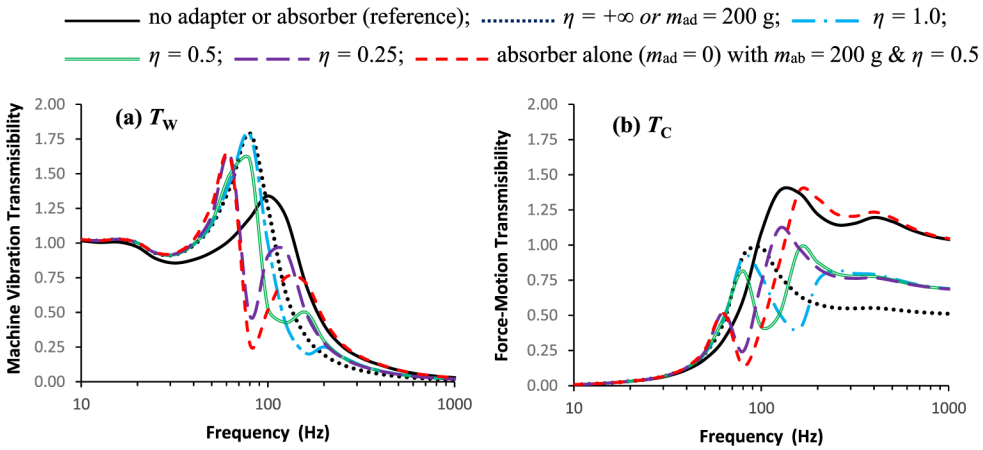

Fig. 11.

The effects of adapter vibration absorber (m_{ad} = 100 g, m_{ab} = 100 g, $K_{ab} = \eta K_1 = 98682\,\eta$, $C_{ab} = \eta C_1 = 32.6\,\eta$) on workpiece vibration predicted using the model shown in Fig. 2(a): (a) machine vibration transmissibility; (b) force-motion transmissibility.

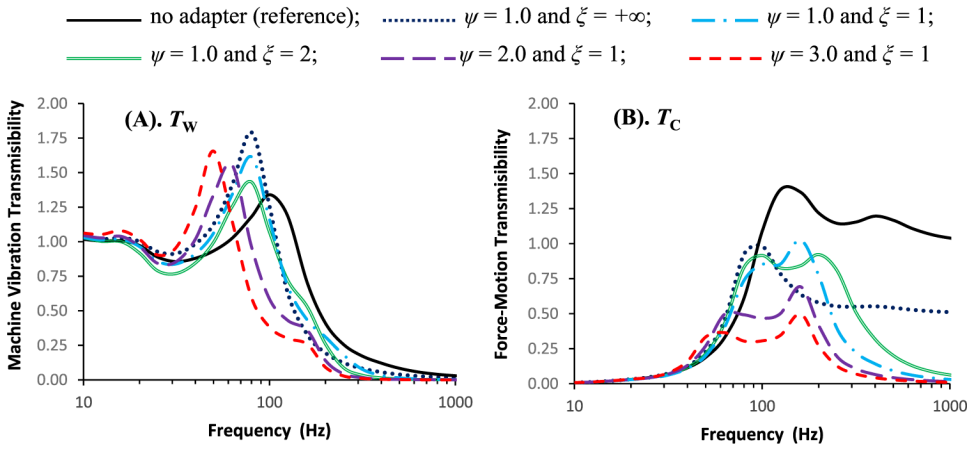

Fig. 12.

The effects of suspended adapter ($m_{ad} = 0.2\psi\ kg \approx \psi m_c$, $K_{ad} = \xi K_1 = 98682\xi$, $C_{ad} = \xi C_1 = 32.6\xi$) on the vibration of the adapter (held by the hands) predicted using the model shown in Fig. 2(b): (A). Machine vibration transmissibility; (B). Cutting vibration transmissibility.

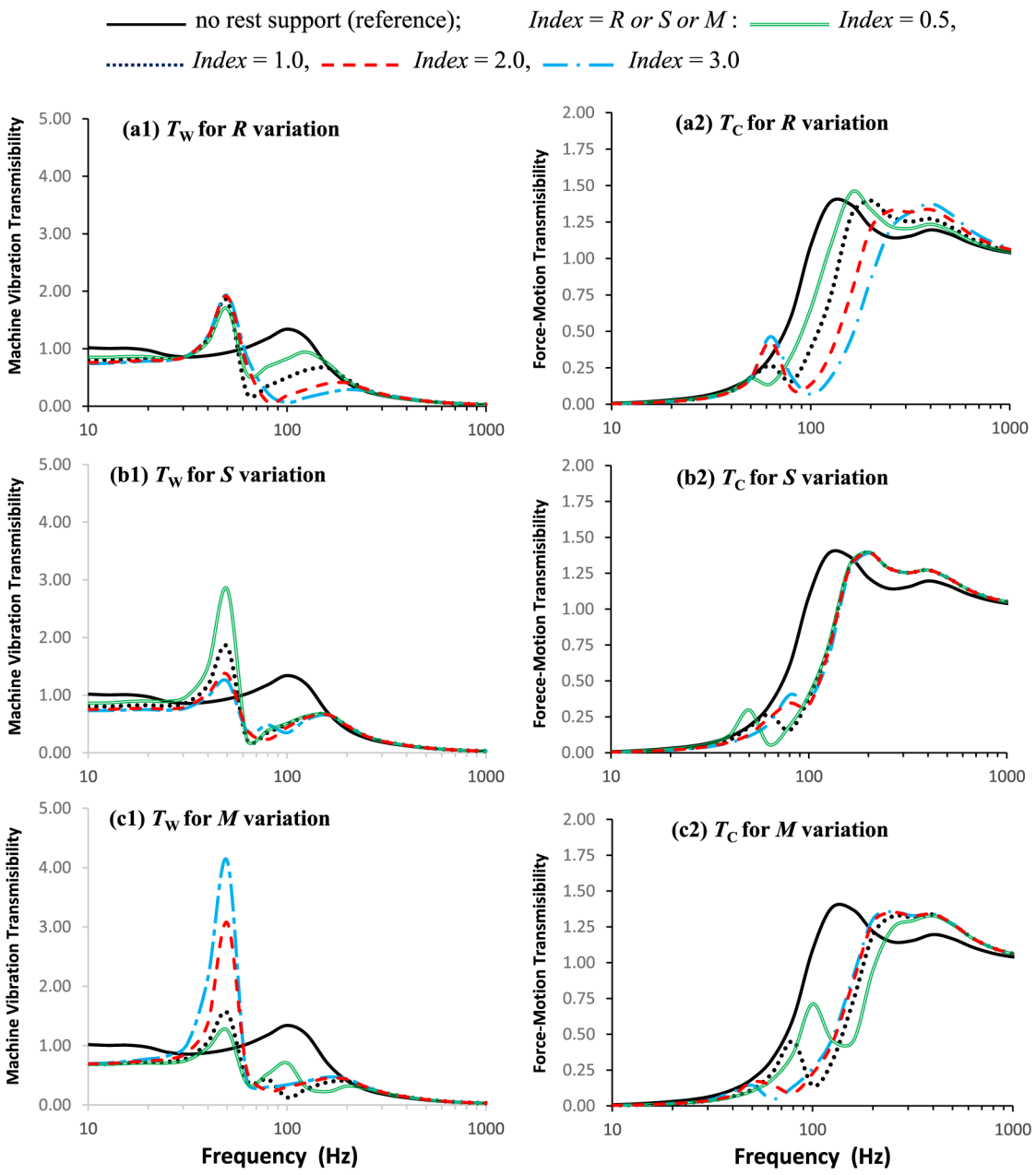

Fig. 13.

The effects of a rest support on workpiece responses predicted using the model shown in Fig. 3(b) with $X = 1$ and $Y = 1$ in the machine body model: (a) the effects of rest contact properties ($K_R = RK_1$, $C_R = RC_1$) for given rest mass and support properties ($M = 1$, $S = 1$); (b) the effects of rest support properties ($K_S = SK_1$, $C_S = SC_1$) for given rest mass and contact properties ($M = 1$, $R = 1$); (c) the effects of rest mass ($m_R = M$ kg) for given rest contact and support properties ($R = 2$, $S = 2$).

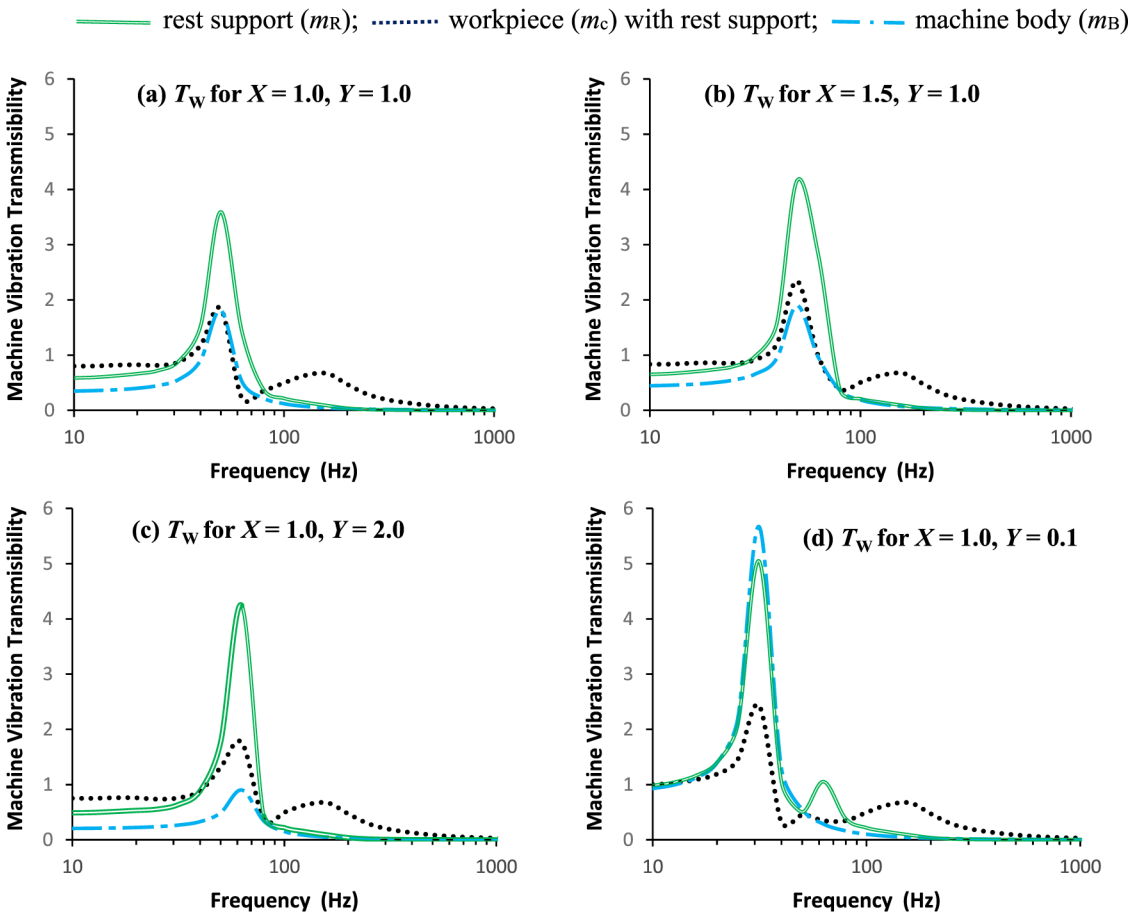

Fig. 14.

The effects of machine dynamic properties on the vibration responses of a workpiece, rest support, and machine body subjected to the excitation acting on the drive wheel (F_w), which were predicted using the model shown in Fig. 3(b) with $R = 1$, $S = 1$, *and* $M = 1$ in the rest support model: (a) $X = 0.5$, $Y = 1$; (b) $X = 1$, $Y = 1$; (c) $X = 2$, $Y = 1$; (d) $X = 1$, Y ′O 2.

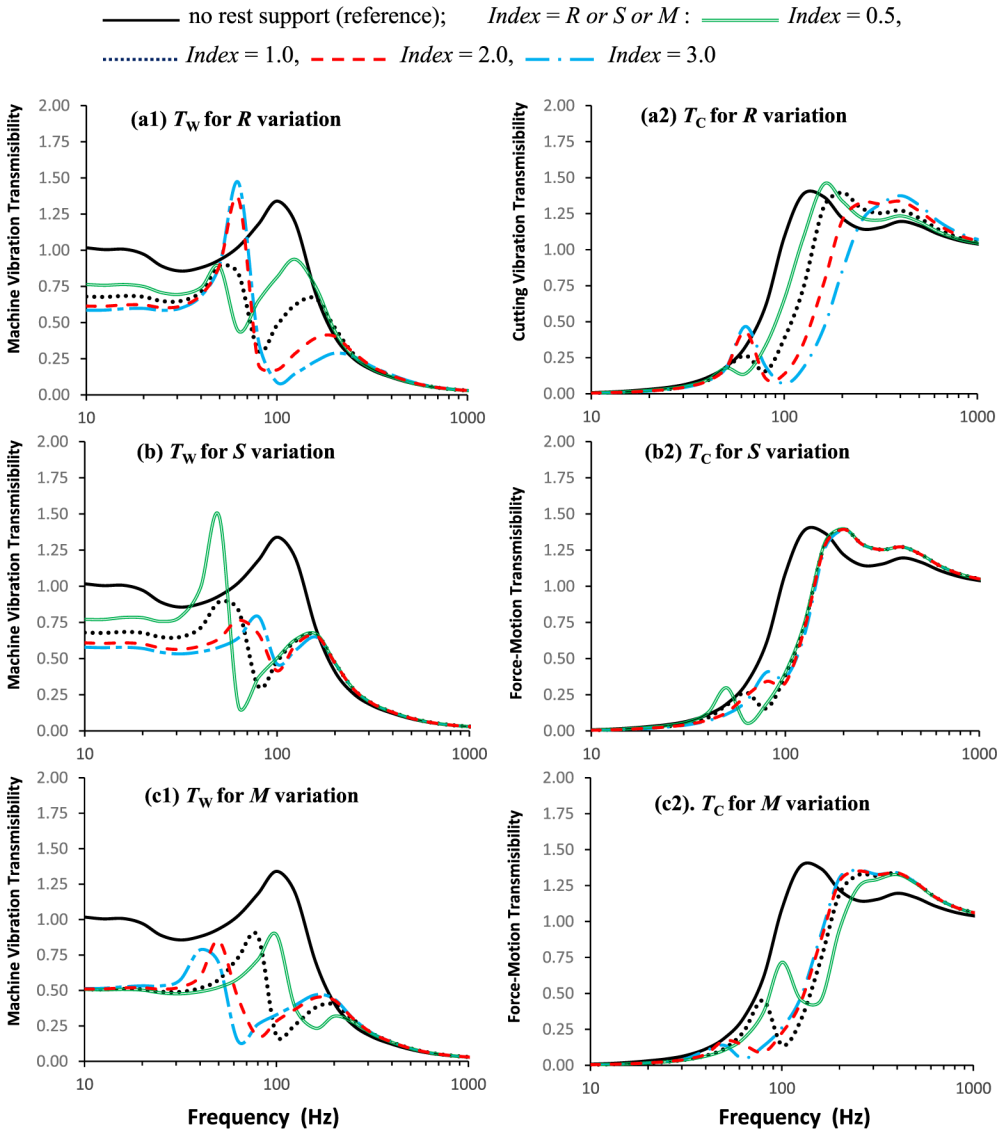

Fig. 15.

The effects of an independent rest support on the workpiece responses predicted using the model shown in Fig. 3(c) with $X = 1$ and $Y = 1$ in the machine body model: (a) the effects of rest contact properties ($K_R = R\,K_1$, $C_R = R\,C_1$) for given rest support mass (m_R = 1.0 kg) and support properties ($K_S = K_1$, $C_S = C_1$); (b) the effects of rest support properties ($K_S = S\,K_1$, $C_S = S\,C_1$) for given rest support mass (m_R = 1.0 kg) and rest contact properties ($K_R = K_1$, $C_R = C_1$); (c) the effects of rest support mass ($m_R = M$ kg) for given rest contact and support properties ($K_R = 2K_1$, $C_R = 2C_1$, $K_S = 2K_1$, $C_S = 2C_1$).

Table 1

The model parameters for six study treatments: a workpiece (golf club head) held by the bare hands with two applied feed forces (15 N and 30 N) on three different grinding interfaces (R45, R55, and R65).

ID		Unit	Feed Force	
			15 N	**30 N**
Hand-Arm System				
m_f		kg	0.043	0.044
m_a		kg	1.425	1.436
m_u		kg	3.216	3.105
K_{f1}		N/m	127,053	210,336
K_{f2}		N/m	16,894	25,878
K_p		N/m	0	0
K_a		N/m	6969	7329
K_u		N/m	4415	3885
C_{f1}		N ·s/m	15.0	20.1
C_{f2}		N ·s/m	58.4	76.1
C_p		N ·s/m	1.8	0.0
C_a		N ·s/m	72.0	86.6
C_u		N ·s/m	82.4	77.7
Workpiece & Grinding Machine				
m_c		kg	0.201	
m_w		kg	19.5	
K_2		N/m	10,000,000	
C_2		N ·s/m	8000	
Grinding Intel faces				
K_1	**R45**	N/m	55,212	63,322
	R55		90,661	98,682
	R65		170,031	230,934
C_1	**R45**	N ·s/m	24.0	14.7
	R55		35.6	32.6
	R65		52.9	60.6
f_c	**R45**	Hz	83	89
	R55		107	112
	R65		146	171

Note: Undamped natural frequency $f_c = \frac{1}{2\pi}\sqrt{K_1/m_c}$

Table 2

The correlations between the workpiece vibrations ($A_{C\text{-}Measured}$) measured at three machine operation speeds (1,200, 1,800, and 2400 rpm) and their corresponding free-run machine body vibrations (A_{MB}) or estimated vibrations ($A_{C\text{-}W}$, $A_{C\text{-}CW}$, $A_{C\text{-}M}$, and $T_C{*}A_{MB}$) with T_W and T_C under three interfaces (R45, R55, and R65) with two feed forces (15 N and 30 N) for ζ/m_c = 2.5.

Correlation Coefficient (*R*-Value)							
Frequency range (Hz)		**20 to 125**			**160 to 1600**		
Operation speed (rpm)		1200	1800	2400	1200	1800	2400
$A_{C\text{-}Measured}$ vs. A_{MB}		0.818	0.283	0.593	0.217	0.173	0.751
Interface R65							
$A_{C\text{-}Measured}$ vs. $A_{C\text{-}W}$	**15 N**	0.925	0.570	0.809	− 0.158	− 0.093	− 0.115
	30 N	0.904	0.505	0.774	− 0.134	− 0.082	− 0.105
$A_{C\text{-}Measured}$ vs. $A_{C\text{-}CW}$	**15 N**	0.940	0.970	0.944	− 0.193	− 0.156	− 0.173
	30 N	0.942	0.974	0.949	− 0.146	− 0.120	− 0.152
$A_{C\text{-}Measured}$ vs. $A_{C\text{-}M}$	**15 N**	0.949	0.944	0.963	− 0.186	− 0.143	− 0.162
	30 N	0.950	0.884	0.950	− 0.143	− 0.112	− 0.142
$A_{C\text{-}Measured}$ vs. ($T_C{*}A_{MB}$)	**15 N**	0.946	0.978	0.958	0.197	0.197	0.731
	30 N	0.948	0.979	0.962	0.253	0.199	0.752
Interface R55							
$A_{C\text{-}Measured}$ vs. $A_{C\text{-}W}$	**15 N**	0.902	0.450	0.691	− 0.128	− 0.023	− 0.042
	30 N	0.890	0.479	0.732	− 0.135	− 0.045	− 0.037
$A_{C\text{-}Measured}$ vs. $A_{C\text{-}CW}$	**15 N**	0.954	0.934	0.971	− 0.159	− 0.052	− 0.086
	30 N	0.951	0.965	0.960	− 0.162	− 0.075	− 0.054
$A_{C\text{-}Measured}$ vs. $A_{C\text{-}M}$	**15 N**	0.967	0.914	0.981	− 0.152	− 0.045	− 0.076
	30 N	0.962	0.942	0.974	− 0.156	− 0.068	− 0.050

Correlation Coefficient (*R*-Value)							
Frequency range (Hz)		**20 to 125**			**160 to 1600**		
$A_{C\text{-}Measured}$ vs. (T_C*A_{MB})	**15 N**	0.954	0.971	0.971	0.206	0.196	0.744
	30 N	0.951	0.978	0.964	0.227	0.190	0.774
Interface R45							
$A_{C\text{-}Measured}$ vs. $A_{C\text{-}W}$	**15 N**	0.718	0.211	0.455	− 0.101	0.019	0.002
	30 N	0.776	0.325	0.576	− 0.141	− 0.056	− 0.065
$A_{C\text{-}Measured}$ vs. $A_{C\text{-}CW}$	**15 N**	0.947	0.826	0.973	− 0.120	0.018	− 0.025
	30 N	0.956	0.878	0.991	− 0.158	− 0.064	− 0.064
$A_{C\text{-}Measured}$ vs. $A_{C\text{-}M}$	**15 N**	0.974	0.755	0.888	− 0.116	0.018	− 0.018
	30 N	0.973	0.842	0.972	− 0.154	− 0.062	− 0.064
$A_{C\text{-}Measured}$ vs. (T_C*A_{MB})	**15 N**	0.964	0.957	0.993	0.214	0.197	0.745
	30 N	0.959	0.965	0.982	0.231	0.191	0.772